Bianisotropic response of microfabricated metamaterials in the terahertz region

Xin-long Xu, Bao-gang Quan, Chang-zhi Gu, and Li Wang

Institute of Physics, Chinese Academy of Sciences, Beijing 100080, China

Received November 14, 2005; revised January 20, 2006; accepted January 20, 2006; posted January 27, 2006 (Doc. ID 65934)

Terahertz time-domain spectroscopy was used to investigate the bianisotropic response of microfabricated split-ring resonators (SRRs) and the in-plane SRR–wire metamaterials. We observed a strong polarization dependence of the transmission with a polarized incident terahertz electromagnetic wave. Two transmission minima, one from the bianisotropic contribution and the other from the anisotropic plasmonic contribution, are discussed. The evolution of the two transmission minima as a function of polarization angle is also demonstrated. The effective-medium theory combined with the dispersion relations in metamaterials is employed to elucidate the experimental data effectively. © 2006 Optical Society of America

OCIS codes: 300.6270, 260.2110, 160.4670, 160.4760.

1. INTRODUCTION

Design and characterization of periodic dielectric or metallic structures such as photonic crystals and metamaterials with unique electromagnetic responses have stimulated extensive attention due to the unusual physical phenomena and the potential applications in optical devices.[1–4] These artifical materials are based on the original concept of manipulating electromagnetic waves by modulating the permittivity (ε) and/or the permeability (μ) of the natural materials. Split-ring resonators (SRRs) and wires were such patterned structures introduced by Pendry *et al.*[5,6] to exhibit negative μ and negative ε simultaneously. Theories and experiments[2–10] have revealed the fascinating electromagnetic properties of this combination, such as reversal Snell's law, reversal Doppler law, reversal Čerenkov radiation, and inversion of critical angle and Brewster angle, etc. Recently, the research of these so-called metamaterials has been pushing forward from the microwave region to the terahertz (THz) region because of not only the verification of the scale invariant, but also because of the potential applications in biological fingerprinting, security imaging, remote sensing, and high-frequency magnetic or electric resonant devices in the THz region.[11–15] Particularly, few natural materials can exhibit magnetic response in the THz region, but the induced current by the THz wave in SRRs can lead to an induced magnetic response. Thus, the SRR as an artificial magnetic metamaterial is useful in the THz region. Recent experimental contributions in the THz region by Yen *et al.*,[11] Wu *et al.*,[12] Linden *et al.*,[13] and Moser *et al.*[14] have opened a window to verify these unusual physical electromagnetic phenomena and to apply the designed devices to new applications in the THz region. Although it is well known that the SRR-based metamaterials are intrinsically anisotropic due to different electromagnetic responses under different orientations of the rings or wires, to our knowledge, it is Marqués *et al.*[16] who first pointed out the existence of bianisotropic effects in these artifical materials at light of the theory of bianisotropic media.

In this paper, we systematically demonstrate THz response of the microfabricated SRR and the in-plane SRR–wire metamaterials by broadband THz time-domain spectroscopy (TDS) in the 0.3–2.5 THz region. The polarization dependence and the evolution of the amplitude transmission for these planar samples are analyzed. It is revealed that there are two transmission minima at different polarization angles, one corresponding to the bianisotropic effect and the other corresponding to the anisotropic plasmonic resonance. With the variation of the polarization of the incident wave, the former vanished and the latter remained almost in the same position. Theoretical analysis using effective-media theory combined with the dispersion relations shows a good agreement with the experimental data. The detailed knowledge of the THz response of SRR and in-plane SRR–wire metamaterials is highly relevant to the development, characterization, and application of these metamaterials in the THz region.

2. EXPERIMENT

SRR and in-plane SRR–wire metamaterials used in our experiments are fabricated by the procedures of photolithography, magnetron sputtering, and lift-off processes. The patterns were deposited with 320 nm depth of copper on quartz slabs. Our quartz substrate is not crystal but is quartz glass (fused silica) with a thickness of 0.8 mm. Figure 1 schematically shows the designed SRR [Fig. 1(a)] and in-plane SRR–wire metamaterials [Fig. 1(b)]. A double-ring SRR used in our experiment is the traditional rectangular pattern with its structure parameters defined as follows: the distance between the internal and external rings, the gaps of the rings, the width of the wire, and the side length of the external rings are 3, 4, 4, and 30 μm, respectively. If the array of the SRR is treated as a peri-

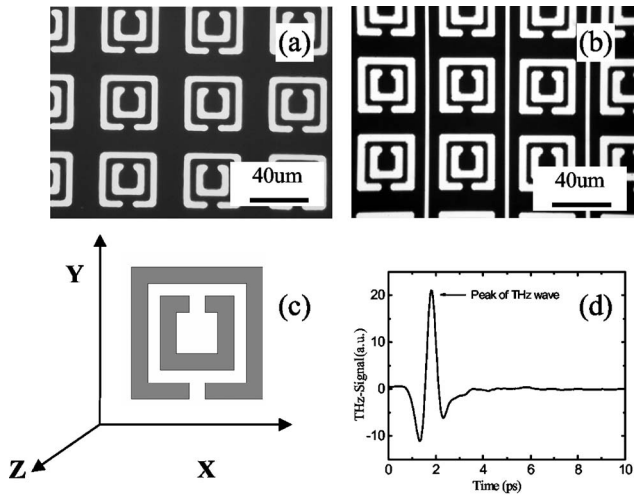

Fig. 1. (a) Schematic of a SRR on a quartz slab. (b) Schematic of in-plane SRR–wire metamaterials on a quartz slab. (c) The Cartesian coordinate system (x,y,z) is chosen in our experiment with the sample located in the x,y plane and the incident wave is along the z axis. The electric vector is along the x axis. The gap-bearing sides of the SRR is along the x axis. (d) Typical THz time-domain wave; the arrow indicates the peak of the THz wave.

odic quadratic lattice, the lattice constant is ~44 μm. The in-plane SRR–wire metamaterials were fabricated with the same structure of the SRR samples. Compared with the SRR samples, one notable difference of the SRR–wire metamaterials is the addition of wires, which are next to the SRR [Fig. 1(b)]. The distance between two wires is ~44 μm and the width of the wires is ~2 μm. To our knowledge, single- and double-ring SRR designs are both standard and conventional SRR structures. Although in the higher frequency such as 100 THz (Ref. 13) the single-ring SRR structure is more feasible considering the difficulty of microfabricating, the double-ring SRR structure is more conventional in the low-frequency region. Also, the double-ring SRR can bring about the coupling of the two individual SRRs and provide a more clear resonance.

Our experimental setup for THz TDS is similar to the systems described in Refs. 17 and 18. THz pulse waves are generated at the front surface of an InAs(110) wafer excited by a mode-locked Ti:sapphire laser (Spectra-Physics Inc.), which is operated at a repetition rate of 82 MHz, a central wavelength of 800 nm, and a pulse duration of 100 fs. The electric components of the THz waves are recorded by electro-optical sampling with ZnTe (110). To avoid the absorption effect of water in the air, all the optical elements, through which THz waves pass, are capsulated in a vacuum chamber.[19] Our spectral resolution is ~0.075 THz, which is determined by the scanning time window of the experiments, and the signal-to-noise ratio can reach approximately 1000:1. Compared with conventional far-infrared Fourier transformation spectroscopy, THz TDS[20] can efficiently extract the amplitude and phase information of the samples without using the Kramers–Kronig relation. All our experiments were done with the THz wave normally incident to the sample plane, and the wave vector **k** is along the z axis [Fig. 1(c)]. The Cartesian coordinate system (x,y,z) is chosen in the experiment as shown in Fig. 1(c). The samples are in the x,y plane with the gap-bearing sides of the SRR lined along the x axis. The linear polarization state of the radiated THz pulse is polarized along the x axis [Fig. 1(c)] with the polarization percentage at approximately 100%. To demonstrate the polarization response of the samples and to simplify our experiments, we rotated the samples along the z axis instead of changing the polarization of the incident wave. They are equivalent manipulations, and in Section (3) we will describe the results as if the samples remain unchanged while the polarization of the incident THz wave is rotated along the z axis. It is easily to see [Fig. 1(c)] that when the electric vector (**E**) of the incident wave is along the x axis, it is a TM mode or a p wave. On the other hand, when **E** is perpendicular to the x axis, it is a TE mode or s wave. Figure 1(d) presents a typical THz time-domain wave. By a fast Fourier transformation of the time-domain wave in the form of $T=t(\omega)\exp[i\Delta\phi(\omega)]$, the frequency-dependent amplitude and phase of the samples are extracted. Here $t(\omega)$ is the amplitude transmission, and $\Delta\phi(\omega)$ is the phase difference between the samples and the quartz substrate.

3. RESULTS

A. Transmission and Polarization Dependence of Split-Ring Resonator Metamaterials

The polarization dependence of a SRR is shown in Fig. 2(a). This response could not be described evidently by a simple sine function with a period of π. This could come from the imperfections in the nanofabrication process that can induce the deviation. The x axis presents the included angle between **E** and the gap-bearing sides of the SRR. The y axis is the monitored peak signal of the THz wave [Fig. 1(d)]. The evolution of the amplitude transmission comes from the fact that when **E** and the gap-bearing sides of the SRR were changed from parallel to vertical, the electric field vector projecting on the x axis in Fig. 1(c) changed periodically. This response really reflects the symmetrical characteristic of the SRR. Figure 2(b) shows the evolution of transmission spectra obtained when the angle between **E** and the gap-bearing sides of the samples is changed from 0° (TM mode) to 90° (TE mode). It is evident that there are two transmission minima in the transmission spectra, one located at ~0.9 THz and the

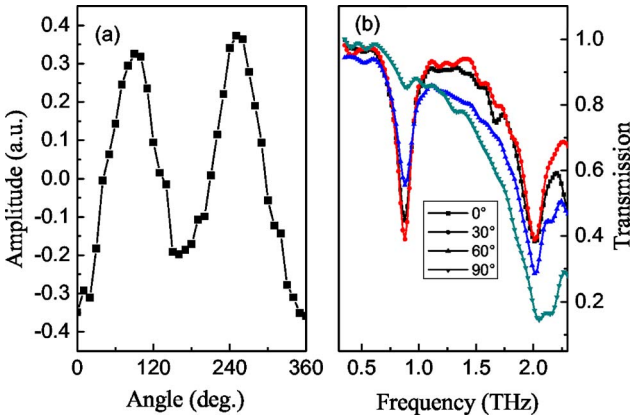

Fig. 2. (Color online) (a) Angular dependence of the transmission of a THz peak signal through the SRR sample. (b) Transmission through the SRR sample as a function of frequency at different polarization orientations (0°, 30°, 60°, and 90°).

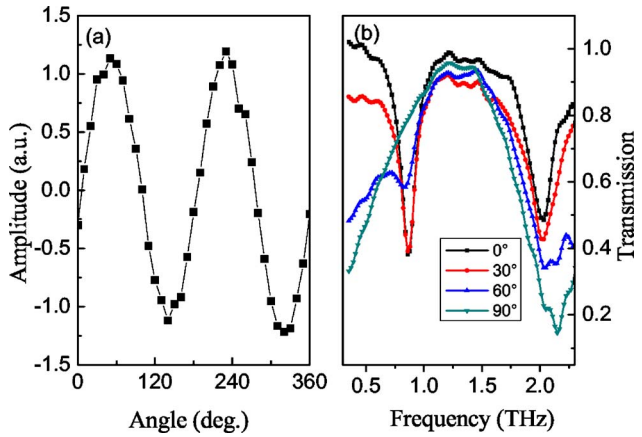

Fig. 3. (Color online) (a) Angular dependence of the transmission of a THz peak signal through the in-plane SRR–wire metamaterials. (b) Transmission through the in-plane SRR–wire metamaterials as a function of frequency at different polarization orientations (0°, 30°, 60°, and 90°).

other located at ~2.1 THz. The first one almost vanished at the angle of 90°, while the second one almost remained in the same position at any rotation angle. The different evolutions of the two transmission minima suggested different responses. As discussed in detail by Marqués *et al.*[16] and Chen *et al.*,[21] the SRR should act not only as a magnetic dipole, but also as an electric dipole. From physical intuition, our observed phenomenon should come from the difference of magnetic and electric dipole responses. Although many works focus on the case that the magnetic vector (**H**) of the incident, wave propagates through the SRR plane, Katsarakis *et al.*[22–24] pointed out that the electric coupling to the magnetic resonance should also exist in the SRR. They emphasized that **E** can couple to **H** when **E** is parallel to the gap-bearing sides of the SRR. In our experimental arrangement, the case of the TM mode satisfied the condition and this, in turn, will lead to the electric coupling to the magnetic resonance. For the case of the TE mode, there is no coupling between **E** and **H**, resulting in the vanishing of magnetic resonance. So the first transmission minimum comes from the magnetic response, and the second transmission minimum comes from the plasmonic resonance for the electric response. The physical properties of the SRR are of crucial relevance to the development of metamaterials, and some more interesting results by experimental, numerical, and analytical methods are put forward.[16,23,25–27] We will employ the effective-medium assumption[23] and the bianisotropic effect[16,21] to discuss our experimental results (in Section (4)), and it may be clear and easy to understand that the first transmission minimum is from the bianisotropic contribution and the second transmission minimum is from the anisotropic plasmonic contribution.

B. Transmission and Polarization Dependence of In-Plane Split-ring Resonator–Wire Metamaterials

Figure 3(a) presents the polarization dependence of the peak signal of a THz wave propagating through the in-plane SRR–wire metamaterials. This response manifests clearly a period of π and represents the symmetrical characteristic of the SRR–wire metamaterials. The data in Fig. 3(b) demonstrate the evolution of transmission spectra when the angle between **E** and the gap-bearing sides of the samples is changed from 0° (TM mode) to 90° (TE mode). The distinguishing features of in-plane SRR–wire metamaterials come from two aspects: one is from wires with the characteristic of low transmission in low frequency for the case of the TE mode and the other is from the SRR with the characteristic of two transmission minima as discussed in the SRR sample. For both the SRR and the SRR–wire metamaterials, we did not observe a remarkable shift of the second transmission minima when the polarization was changed. To our knowledge, there may be two main aspects for this. One is the imperfections in the nanofabrication process that can induce the minor deviation and the other may be that the difference in the effective electron density is so small when the orientation of the SRRs is changed from 0 to 90 deg, that our system cannot differentiate this change.

4. THEORY AND DISCUSSION

A. Effective-medium Assumption and Bianisotropic Description

The theoretical and experimental concept of SRR-based metamaterials is grounded on the effective-medium assumption. Under this description, the unit cell of a periodic structure has dimensions significantly smaller than the probing wavelength, and the macroscopical description of materials such as the electric permittivity and the magnetic permeability is feasible. For example, if the probing electromagnetic wave posseses the frequency ω and the wavelength $\lambda = 2\pi c/\omega$ (c is the velocity of the electromagnetic wave in vacuum), the dimensions of the unit cell of the artificial material should hold the conditions[5] $d \ll \lambda$. In our experimental condition, $d \approx 44\ \mu$m, and $\lambda_{1\ \mathrm{THz}} \approx 300\ \mu$m can satisfy this restriction. Under the frame work of the effective-medium theory,[23] SRRs have a strong electric response equivalent to an electric dipole and a strong magnetic response equivalent to a magnetic dipole. The analytical expressions for the effective parameters of SRR-based structures are also discussed in Ref. 23.

As described by Marqués *et al.*[16] in detail, the bianisotropy is related to the existence of magnetic and electric coupling in the artificial constituents of the materials. In our experimental arrangement [Fig. 1(c)], the z component of the magnetic field can produce an electric dipole in the x direction and the x component of the electric field can produce a magnetic dipole in the y direction. Thus the bianisotropic terms in SRRs cannot be neglected. Under the reciprocal assumption,[16,21,28,29] the constitutive relationships of the SRR-based metamaterials read as follows:

$$\mathbf{D} = \varepsilon_0 \bar{\bar{\varepsilon}} \mathbf{E} + \frac{1}{c} \bar{\bar{\xi}} \mathbf{H}, \tag{1a}$$

$$\mathbf{B} = \mu_0 \bar{\bar{\mu}} \mathbf{H} + \frac{1}{c} \bar{\bar{\chi}} \mathbf{E}, \tag{1b}$$

where ε_0 and μ_0 are the permittivity and permeability in vacuum, respectively. $c = 1/\sqrt{\varepsilon_0 \mu_0}$ is the velocity of the

electromagnetic wave in vacuum, $\bar{\bar{\varepsilon}}$ and $\bar{\bar{\mu}}$ are the relative permittivity and permeability in the form of tensors. $\bar{\bar{\xi}}$ and $\bar{\bar{\chi}}$ describe the coupling of the magnetic and electric fields and these will yield the unique physics in SRRs.

B. Dispersion Relations, Transmission, and Reflection Coefficients

The interaction of the electromagnetic wave with the SRR-based metamaterials is determined by the dispersion relations, transmission, and reflection coefficients at the boundary. Here we adopt the method presented in Ref. 28. Let us consider a plane-wave solution with the form of $\exp[i(\mathbf{k}\cdot\mathbf{r}-\omega t)]$. Thus the Maxwell equations can be expressed as

$$\mathbf{k}\times\mathbf{E}=\omega\mathbf{B}, \tag{2a}$$

$$\mathbf{k}\times\mathbf{H}=-\omega\mathbf{D}, \tag{2b}$$

$$\mathbf{k}\cdot\mathbf{B}=0, \tag{2c}$$

$$\mathbf{k}\cdot\mathbf{D}=0, \tag{2d}$$

where $\mathbf{k}$ is the wave vector, and in vacuum $k=\omega/c=\sqrt{\varepsilon_0\mu_0}\omega$. After eliminating the magnetic vector $\mathbf{H}$, Eqs. (1) and (2) can be transformed as the following equation:

$$\left[\frac{\omega^2}{c^2}\left(\bar{\bar{\varepsilon}}-\bar{\bar{\xi}}\bar{\bar{\mu}}^{-1}\bar{\bar{\chi}}\right)+\frac{\omega}{c}\left(\bar{\bar{\xi}}\bar{\bar{\mu}}^{-1}\cdot k\bar{\bar{K}}-k\bar{\bar{K}}\cdot\bar{\bar{\mu}}^{-1}\bar{\bar{\xi}}\right)+k\bar{\bar{K}}\cdot\bar{\bar{\mu}}^{-1}k\bar{\bar{K}}\right]\cdot\mathbf{E}=0, \tag{3}$$

where

$$k\bar{\bar{K}}=\begin{bmatrix}0 & -k_z & k_y\\ k_z & 0 & -k_x\\ -k_y & k_x & 0\end{bmatrix}. \tag{4}$$

To obtain the nonzero solution of $\mathbf{E}$, the determinant of Eq. (3) should be zero. If the diagonalizable tensors of Eqs. (1) are expressed as

$$\bar{\bar{\varepsilon}}=\begin{bmatrix}\varepsilon_{xx} & 0 & 0\\ 0 & \varepsilon_{yy} & 0\\ 0 & 0 & \varepsilon_{zz}\end{bmatrix},\quad \bar{\bar{\mu}}=\begin{bmatrix}\mu_{xx} & 0 & 0\\ 0 & \mu_{yy} & 0\\ 0 & 0 & \mu_{zz}\end{bmatrix},$$

$$\bar{\bar{\xi}}=\begin{bmatrix}0 & 0 & -i\xi_{xz}\\ 0 & 0 & 0\\ 0 & 0 & 0\end{bmatrix},\quad \bar{\bar{\chi}}=\begin{bmatrix}0 & 0 & 0\\ 0 & 0 & 0\\ i\xi_{xz} & 0 & 0\end{bmatrix}, \tag{5}$$

the determinant satisfies the following equation:

$$\begin{bmatrix}\frac{\omega^2\varepsilon_{xx}}{c^2}-\frac{\omega^2\xi_{xz}^2}{c^2\mu_{zz}}-\frac{k_z^2}{\mu_{yy}}-\frac{k_y^2}{\mu_{zz}}, & \frac{k_xk_y}{\mu_{zz}}-i\frac{\omega k_x\xi_{xz}}{c\mu_{zz}}, & \frac{k_xk_z}{\mu_{yy}}\\ \frac{k_xk_y}{\mu_{zz}}+i\frac{\omega k_x\xi_{xz}}{c\mu_{zz}}, & \frac{\omega^2\varepsilon_{yy}}{c^2}-\frac{k_z^2}{\mu_{xx}}-\frac{k_x^2}{\mu_{zz}}, & \frac{k_yk_z}{\mu_{xx}}\\ \frac{k_xk_z}{\mu_{yy}}, & \frac{k_yk_z}{\mu_{xx}}, & \frac{\omega^2\varepsilon_{zz}}{c^2}-\frac{k_y^2}{\mu_{xx}}-\frac{k_x^2}{\mu_{yy}}\end{bmatrix}=0. \tag{6}$$

In our experimental arrangements [Fig. 1(c)], we can see that SRR and in-plane SRR–wire metamaterials possess the bianisotropy between the x and z axes and this is described in ξ_{xz}. Then Eq. (6) fulfills the equations as follows:

$$k_z^2=\frac{\omega^2}{c^2}\varepsilon_{yy}\mu_{xx}, \tag{7}$$

$$k_z^2=\frac{\omega^2}{c^2}\varepsilon_{xx}\mu_{yy}-\frac{\omega^2\mu_{yy}}{c^2\mu_{zz}}\xi_{xz}^2, \tag{8}$$

where Eq. (7) is the dispersion relation for the TE mode in metamaterials and Eq. (8) stands for the dispersion relation for the TM mode. From these equations, it is evident that the TE mode totally comes from the response of ε_{yy} (μ_{xx} is equal to 1 for nonmagnetic materials) and the TM mode comes from two factors: one is ε_{xx} for the electric dipole and the other is ξ_{xz} for the bianisotropic contribution due to the electric coupling to the magnetic response.

The transmission and reflection coefficients are determined by the boundary condition of the Maxwell equations. Because an arbitrary polarized wave can be decomposed into TE and TM modes,[28] we discuss TE and TM modes only. For the TE mode, the incidence, reflection, and transmission of the electric vector under the coordinate in Fig. 1(c) can be written as

$$\mathbf{E_i}=\hat{y}E_0e^{ik_xx+ik_zz}, \tag{9}$$

$$\mathbf{E_r}=\hat{y}R^{\mathrm{TE}}E_0e^{ik_{rx}x-ik_{rz}z}, \tag{10}$$

$$\mathbf{E_t}=\hat{y}T^{\mathrm{TE}}E_0e^{ik_{tx}x+ik_{tz}z}, \tag{11}$$

where E_0 is the amplitude of the incident wave. R^{TE} and T^{TE} are the reflection and transmission coefficients, respectively. By applying Eqs. (1) and (2), the magnetic vector can be reformed as

$$\mathbf{H_i} = -\hat{x}\frac{k_z E_0}{\mu_0 \omega} e^{ik_x x + ik_z z} + \hat{z}\frac{k_x E_0}{\mu_0 \omega} e^{ik_x x + ik_z z}, \tag{12}$$

$$\mathbf{H_r} = \hat{x}\frac{k_{rz} E_0}{\mu_0 \omega} R^{\mathrm{TE}} e^{ik_{rx} x - ik_{rz} z} + \hat{z}\frac{k_{rx} E_0}{\mu_0 \omega} R^{\mathrm{TE}} e^{ik_{rx} x - ik_{rz} z}, \tag{13}$$

$$\mathbf{H_t} = -\hat{x}\frac{k_{tz} E_0}{\mu_0 \mu_{xx} \omega} T^{\mathrm{TE}} e^{ik_{tx} x + ik_{tz} z} + \hat{z}\frac{k_{tx} E_0}{\mu_0 \mu_{zz} \omega} T^{\mathrm{TE}} e^{ik_{tx} x + ik_{tz} z}. \tag{14}$$

At $z=0$, the electric and the magnetic vectors should fulfill the boundary condition:

$$\mathbf{n} \times (\mathbf{E}_1 - \mathbf{E}_2) = 0, \tag{15a}$$

$$\mathbf{n} \times (\mathbf{H}_1 - \mathbf{H}_2) = 0. \tag{15b}$$

Let us combine Eqs. (9)–(15), and then the following equations should be satisfied:

$$T^{\mathrm{TE}} = \frac{2}{1 + k_{tz}/(k_0 \mu_{xx})}, \tag{16}$$

$$R^{\mathrm{TE}} = 1 - \frac{2}{1 + k_{tz}/(k_0 \mu_{xx})}. \tag{17}$$

Because of the duality of the electromagnetic waves,[28] the TM mode can be expressed as

$$T^{\mathrm{TM}} = \frac{2}{1 + k_{tz}/(k_0 \varepsilon_{xx})}, \tag{18}$$

$$R^{\mathrm{TE}} = 1 - \frac{2}{1 + k_{tz}/(k_0 \varepsilon_{xx})}. \tag{19}$$

After substituting the dispersion relations of Eqs. (7) and (8) into Eqs. (16)–(19), we can get

$$T^{\mathrm{TE}} = 2\mu_{xx}/(\mu_{xx} + \sqrt{\varepsilon_{yy}\mu_{xx}}), \tag{20}$$

$$T^{\mathrm{TM}} = 2\varepsilon_{xx} \Bigg/ \left(\varepsilon_{xx} + \sqrt{\varepsilon_{xx}\mu_{yy} - \frac{\mu_{yy}}{\mu_{zz}}\xi_{xz}^2}\right), \tag{21}$$

$$R^{\mathrm{TE}} = 1 - 2\mu_{xx}/(\mu_{xx} + \sqrt{\varepsilon_{yy}\mu_{xx}}), \tag{22}$$

$$R^{\mathrm{TM}} = 1 - 2\varepsilon_{xx} \Bigg/ \left(\varepsilon_{xx} + \sqrt{\varepsilon_{xx}\mu_{yy} - \frac{\mu_{yy}}{\mu_{zz}}\xi_{xz}^2}\right). \tag{23}$$

C. Simulation of the Transmission Evolution

Considering both our experimental arrangements and the effective-medium theory,[21] the frequency-dependent permittivity, permeability, and the coupling of magnetic and electric vectors for the SRR can be expressed as

$$\mu_{xx} = \mu_{yy} = \mu_{zz} = 1, \quad \varepsilon_{xx}(\omega) = \varepsilon_{xx0} - \frac{\omega_{p1}^2 - \omega_{01}^2}{\omega^2 - \omega_{01}^2 + i\omega\gamma_1},$$

$$\varepsilon_{yy}(\omega) = \varepsilon_{yy0} - \frac{\omega_{p2}^2 - \omega_{02}^2}{\omega^2 - \omega_{02}^2 + i\omega\gamma_2},$$

$$\xi_{xz}(\omega) = \xi_{xz0} - \frac{\omega_{m1}^2 - \omega_{m2}^2}{\omega^2 - \omega_{m2}^2 + i\omega\gamma_3}, \tag{24}$$

where ε_{xx0}, ε_{yy0}, ξ_{xz0} are the constants at high frequency. γ_1, γ_2, γ_3 are the damping constants. ω_{01}, ω_{02}, ω_{p1}, ω_{p2}, ω_{m1}, and ω_{m2} are the resonant frequencies. For the in-plane SRR–wire metamaterials, the major difference with the SRR samples is that wires are put together with the SRR, and the wires exhibits the frequency-dependent plasmonic form as[21]

$$\varepsilon^{\mathrm{wire}}(\omega) = \varepsilon_0^{\mathrm{wire}} - \omega_{p3}^2/(\omega^2 + i\omega\gamma_4). \tag{25}$$

Accordingly, the physical parameters have the same meanings as in Eqs. (24), where $\varepsilon^{\mathrm{wire}}(\omega)$ should be negative below ω_{p3}, and hence the transmission is low in the region below ω_{p3}. Using Eqs. (20), (21), (24), (25), and the parameters listed in Table 1, we can simulate the transmission evolution of SRR and in-plane SSR-wire metamaterials effectively. The parameters are chosen according to the experimental data and can then be adjusted in detail. Figure 4 presents the transmission evaluation of a SRR. To view clearly, the simulated transmission in Fig. 4 has been normalized to the maximum values. The bianisotropic response of the first transmission minimum comes from ξ_{xz} due to the coupling of magnetic and electric components in the TM mode, while in the TE mode, ξ_{xz} vanishes and results in the vanishing of the magnetic resonance. The electric resonance comes from two factors: one is ε_{xx} and the other is ε_{yy}. They are different due to the anisotropic properties of the SRR. As for the in-plane SRR–wire metamaterials (Fig. 5), the characteristics of the transmission evolution contain two elements. One is from the SRR and agrees with the SRR samples with the characteristic of electric and magnetic resonances. The other comes from wires. For metallic wires, when the electric vector is along the wire axis, the electrons in the wires can be driven along the wires effectively, and this can result in a low transmission. On the other hand, when the electric vector is vertical to the wire axis, the electrons in the wires cannot move effectively along the wires

Table 1. Theoretical Simulation Parameters for the Data Presented in Figs. 4 and 5[a]

	Parameters (THz)										
	ω_{p1}	ω_{01}	ω_{p2}	ω_{02}	ω_{m1}	ω_{m2}	ω_{p3}	γ_1	γ_2	γ_3	γ_4
Value	2.75	0.97	4.52	2.13	3.28	0.89	0.78	0.36	0.03	0.21	0.50

[a]All parameters should be multipled by 2π.

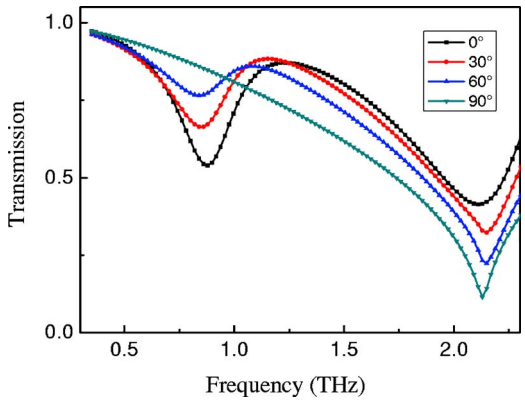

Fig. 4. (Color online) Simulation of the transmission through the SRR sample as a function of frequency at different polarization orientations (0°, 30°, 60°, and 90°).

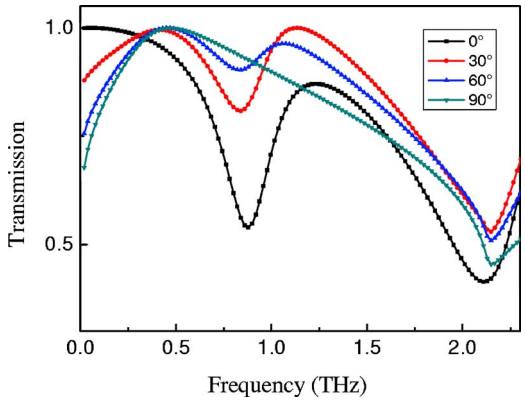

Fig. 5. (Color online) Simulation of the transmission through the in-plane SRR–wire metamaterials as a function of frequency at different polarization orientations (0°, 30°, 60°, and 90°).

and this can in turn bring a high transmission. In the experiment, the defects in samples and the influence of the substrate may bring about some fluctuations in the measured transmission curves.

5. CONCLUSIONS

We presented our recent spectral measurements of the SRR and in-plane SRR–wire metamaterials by THz TDS. All the samples were fabricated by the photolithographic technique in micrometer dimensions. The results showed a strong polarization dependence. Two transmission minima that came from different physical mechanisms are analyzed. The evolution of the two transmission minima can be used to differentiate the electric dipole response and bianisotropy-induced magnetic response. We combine the effective-medium theory with the dispersion conditions to simulate the transmission response of the metamaterials effectively. The detailed knowledge of the bianisotropic responses is highly relevant to the development, characterization, and application of metamaterials in the THz region.

ACKNOWLEDGMENTS

The authors thank Zheng Cui for proofreading this paper. This work was supported by National Natural Science Foundation of China (grants 10390160 and 39890390), the State Key Development Program for Basic Research of China (grant 2002CB613500), and the National Center for Nanoscience and Technology, China.

REFERENCES

1. K. Inoue and K. Ohtaka, *Photonic Crystals: Physics, Fabrication and Applications* (Springer, 2004).
2. V. G. Veselago, "The electrodynamics of substances with simultaneously negative values of ε and μ," Sov. Phys. Usp. **10**, 509–514 (1968).
3. D. R. Smith, P. Kolinko, and D. Schurig, "Negative refraction in indefinite media," J. Opt. Soc. Am. B **21**, 1032–1043 (2004).
4. J. B. Pendry, "Negative refraction makes a perfect lens," Phys. Rev. Lett. **85**, 3966–3969 (2000).
5. J. B. Pendry, A. J. Holden, D. J. Robbins, and W. J. Stewart, "Magnetism from conductors and enhanced nonlinear phenomena," IEEE Trans. Microwave Theory Tech. **47**, 2075–2084 (1999).
6. J. B. Pendry, A. J. Holden, W. J. Stewart, and I. Youngs, "Extremely low frequency plasmons in metallic mesostructures," Phys. Rev. Lett. **76**, 4773–4776 (1996).
7. D. R. Smith, W. J. Padilla, D. C. Vier, S. C. Nemat-Nasser, and S. Schultz, "Composite medium with simultaneously negative permeability and permittivity," Phys. Rev. Lett. **84**, 4184–4187 (2000).
8. R. A. Shelby, D. R. Smith, and S. Schultz, "Experimental verification of a negative index of refraction," Science **292**, 77–79 (2001).
9. C. G. Parazzoli, R. B. Greegor, K. Li, B. E. C. Koltenbah, and M. Tanielian, "Experimental verification and simulation of negative index of refraction using Snell's law," Phys. Rev. Lett. **90**, 107401-1–107401-4 (2003).
10. T. M. Grzegorczyk, Z. M. Thomas, and J. A. Kong, "Inversion of critical angle and Brewster angle in anisotropic left-handed metamaterials," Appl. Phys. Lett. **86**, 251909-1–251909-3 (2005).
11. T. J. Yen, W. J. Padilla, N. Fang, D. C. Vier, D. R. Smith, J. B. Pendry, D. N. Basov, and X. Zhang, "Terahertz magnetic response from artificial materials," Science **303**, 1494–1496 (2004).
12. D. M. Wu, N. Fang, C. Sun, and X. Zhang, "Terahertz plasmonic high pass filter," Appl. Phys. Lett. **83**, 201–203 (2003).
13. S. Linden, C. Enkrich, M. Wegener, J. F. Zhou, T. Koschny, and C. M. Soukoulis, "Magnetic response of metamaterials at 100 THz," Science **306**, 1351–1353 (2004).
14. H. O. Moser, B. D. F. Casse, O. Wilhelmi, and B. T. Saw, "Terahertz response of a microfabricated rod-split-ring-resonator electromagnetic metamaterial," Phys. Rev. Lett. **94**, 063901-1–063901-4 (2005).
15. B. Ferguson and X.-C. Zhang, "Materials for terahertz science and technology," Nat. Mater. **1**, 26–33 (2002).
16. R. Marqués, F. Medina, and R. Rafii-El-Idrissi, "Role of bianisotropy in negative permeability and left-handed metamaterials," Phys. Rev. B **65**, 144440-1–144440-6 (2002).
17. D. Grischkowsky, S. Keiding, M. Van Exter, and Ch. Fattinger, "Far-infrared time-domain spectroscopy with terahertz beams of dielectrics and semiconductors," J. Opt. Soc. Am. B **7**, 2006–2014 (1990).
18. M. Schall, M. Walther, and P. U. Jepsen, "Fundamental and second-order phonon processes in CdTe and ZnTe," Phys. Rev. B **64**, 094301-1–094301-5 (2001).
19. M. V. Exter, C. Fattinger, and D. Grischkowsky, "Terahertz time-domain spectroscopy of water vapor," Opt. Lett. **14**, 1128–1130 (1989).
20. P. Y. Han, M. Tani, M. Usami, S. Kono, R. Kersting, and X.-C. Zhang, "A direct comparison between terahertz time-domain spectroscopy and far-infrared Fourier transform spectroscopy," J. Appl. Phys. **89**, 2357–2359 (2001).
21. X. Chen, B.-I. Wu, J. A. Kong, and T. M. Grzegorczyk,

"Retrieval of the effective constitutive parameters of bianisotropic metamaterials," Phys. Rev. E **71**, 046610-1–046610-9 (2005).
22. N. Katsarakis, T. Koschny, M. Kafesaki, E. N. Economou, and C. M. Soukoulis, "Electric coupling to the magnetic resonance of split ring resonators," Appl. Phys. Lett. **84**, 2943–2945 (2004).
23. T. Koschny, M. Kafesakis, E. N. Economou, and C. M. Soukoulis, "Effective medium theory of left-handed materials," Phys. Rev. Lett. **93**, 107402-1–107402-4 (2004).
24. N. Katsarakis, G. Konstantinidis, A. Kostopoulos, R. S. Penciu, T. F. Gundogdu, Th. Koschny, M. Kafesaki, E. N. Economou, and C. M. Soukoulis, "Magnetic response of split-ring resonators in the far-infrared frequency regime," Opt. Lett. **30**, 1348–1350 (2005).
25. P. Gay-Balmaz and O. J. F. Martin, "Electromagnetic resonances in individual and coupled split-ring resonators," J. Appl. Phys. **92**, 2929–2936 (2002).
26. M. Shamonin, E. Shamonina, V. Kalinin, and L. Solymar, "Properties of a metamaterial element: analytical solutions and numerical simulations for a singly split double ring," J. Appl. Phys. **95**, 3778–3784 (2004).
27. Y.-J. Hsu, Y.-C. Huang, J.-S. Lih, and J.-L. Chern, "Electromagnetic resonance in deformed split ring resonators of left-handed meta-materials," J. Appl. Phys. **96**, 1979–1982 (2004).
28. J. A. Kong, *Electromagnetic Wave Theory* (Wiley, 1975).
29. T. M. Grzegorcyk, X. Chen, J. Pacheco, Jr., J. Chen, B.-I. Wu, and J. A. Kong, "Reflection coefficients and Goos-Hänchen shifts in anisotropic and bianisotropic left-handed metamaterials," Prog. Electromagn. Res. **51**, 83–113 (2005).